

Redshift of acoustic waves in acoustic streaming

Masanori Sato*

Honda Electronics Co., Ltd., 20 Oyamazuka, Oiwa-cho, Toyohashi, Aichi 441-3193, Japan

Tsuyoshi Matsuo

Department of Information Engineering, Toyohashi University of Technology, Hibari-ga-oka, Tempaku-cho, Toyohashi, Aichi 441-8580, Japan

Toshitaka Fujii

Aichi University of Technology, 50-2 Manori, Nishihazama-cho, Gamagori, Aichi 443-0047, Japan

(Received 14 May 2001; revised manuscript received 25 November 2002; published 11 July 2003)

Redshift, namely, the frequency decline in the frequency spectrum of an acoustic wave in water, was observed by measuring the frequency spectrum of acoustic streaming in a standing wave field. We desire that relations of the energy ε and momentum μ of acoustic waves analogous to those under quantum conditions hold, that is, $\varepsilon = n_p \hbar \omega$, $\mu = n_p \hbar k$, where $\hbar = h/2\pi$ (h is Planck's constant), n_p is the phonon density, ω is the angular frequency, and k is the wave number. In this case, a redshift indicates that acoustic waves suffer energy loss or annihilation of phonons. We show that the driving force of streaming is derived from the momentum transfer of phonons and the direct conversion of energy from acoustic energy to kinetic energy of the medium.

DOI: 10.1103/PhysRevE.68.016301

PACS number(s): 43.25.+y, 43.35.+d, 03.65.-w

I. INTRODUCTION

In investigations of liquid ^4He [1,2] and solids [3], acoustic waves are treated as phonons. We have been attempting to investigate the nonlinear phenomena (subharmonics [4], capillary waves [5] and cavitation [6]) of acoustic waves in water using the phonon scheme and quantum mechanics [4–11]. We have treated acoustic waves from the viewpoint of the energy and momentum of phonons [4–11].

Acoustic waves in water have been analyzed on the basis of hydrodynamics [12–15], which is an approximation of the kinetic theory [16]. In hydrodynamics, a Maxwell velocity distribution of the medium particles is assumed, using the medium temperature [16]. Moreover, an approximation to the kinetic theory is obtained by using the velocity distribution function, instead of calculating all the particles' orbits [16]. Thus, the kinetic theory can be used to treat phenomena that are caused by the deformation of the velocity distribution function, such as Landau damping [16], which cannot be explained on the basis of hydrodynamics. However, the redshift of the acoustic wave frequency cannot be explained using hydrodynamics or kinetic theory.

In quantum mechanics, energy is represented by frequency; hence, a redshift indicates energy decline. In acoustic waves, a frequency change known as the Doppler shift occurs, which is a change in the energy density as a result of the motion of the sound source, but it does not imply an energy transfer to the kinetic energy of the medium. The redshift of acoustic waves is not similar to the Doppler shift. The redshift indicates acoustic energy transfer to the kinetic energy of the medium, which causes acoustic streaming [8,9]. This phenomenon is very similar to the Compton effect.

In this paper, we present experimental data on redshift in acoustic streaming. A quantum-mechanical representation of acoustic waves and a mechanism for the redshift are proposed.

II. EXPERIMENT

Figure 1 shows the experimental setup (the water bath dimensions are 190 mm ϕ and 1100 mm depth). Ultrasonic waves from an ultrasonic vibrator are detected using a piezoceramic hydrophone (4 mm ϕ), and the frequency spectrum is analyzed. The ultrasonic vibrators used are piezoceramic disks (50 mm ϕ , 2–3.5 mm thick) and are driven at frequencies of $\omega/2\pi = 500$ –1050 kHz.

Figure 2 shows the experimental setup for detecting the average velocity of acoustic streaming. The average velocity of water (volume of 2.7 l) is measured based on the rotation speed of a rotor. The fins of the rotor are driven by the streaming. The rotation speed of the rotor did not depend critically on the depth of the fins, which indicates that the fins were driven by the streaming of the water and not by acoustic radiation pressure. In these experiments, acoustic streaming which occurred in the standing wave fields depended on the dimensions of the water tank and the water depth.

When acoustic streaming occurs, the lower sideband of the driving frequency is detected. Figure 3(a) shows the frequency spectrum in the absence of acoustic streaming, at a driving voltage of the ultrasonic vibrator $V_{\text{in}} = 9 V_{\text{peak to peak}}$ and a driving frequency of 580 kHz. Figure 3(b) shows the frequency spectrum when there is acoustic streaming. Redshift of the frequency spectrum, with a bandwidth of more than 3 kHz, is shown in Fig. 3(b) at $V_{\text{in}} = 90 V_{\text{peak to peak}}$. The redshift peak frequency f_{peak} is detected as shown in Fig. 3(c) at $V_{\text{in}} = 90 V_{\text{peak to peak}}$. Figures 3(b) and 3(c) were detected under standing wave conditions. The difference in ex-

*Email address: msato@honda-el.co.jp

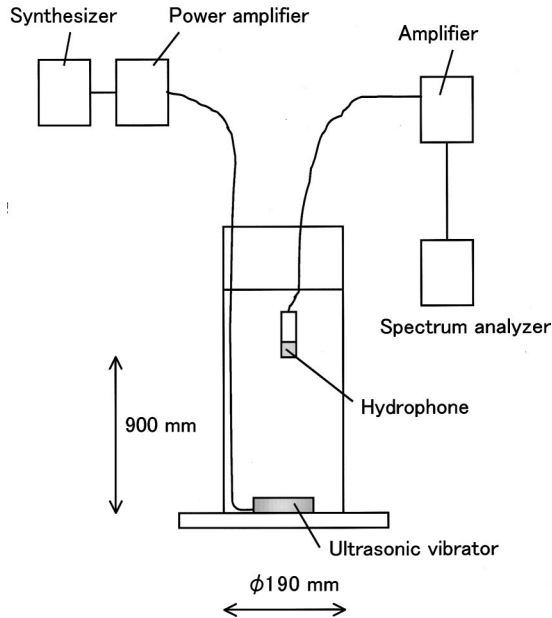


FIG. 1. Experimental setup. The ultrasonic vibrator and the hydrophone are fixed to the water bath; thus the Doppler shift cannot be detected. Water bath dimensions are 190 mm diameter and 1100 mm depth. The hydrophone was set approximately 900 mm from the bottom. The acoustic wave field was a standing wave field, and data were detected after the transient phenomena were complete.

perimental conditions between (b) and (c) is the position of the hydrophone. (However, these two positions were very close, set approximately 900 mm from the bottom; see Sec. III E.) Figure 4 shows the frequency and power dependence of the difference between the driving frequency f_0 and redshift peak frequency f_{peak} ($\Delta f_{\text{peak}} \equiv f_0 - f_{\text{peak}} = \Delta \omega_{\text{peak}} / 2\pi$). Here, Δf_{peak} increases with the driving frequency f_0 . Figure 5 shows the frequency and power dependence of the averaged acoustic streaming velocity, i.e., the averaged volume flow, which is measured from the rotation speed of the rotor.

The ultrasonic vibrator and the hydrophone are fixed to the water bath; thus the Doppler shift cannot be detected after the acoustic streaming stabilizes. These data were measured under standing wave conditions so that transient phenomena were not detected. We did not detect a redshift in agar where no kinetic energy transfer to the medium occurs; we also did not detect a redshift in agar when acoustic energy is transferred to the thermal energy of the medium. In this experiment, the temperature of the agar rose rapidly. Furthermore, we did not detect a redshift in agar when a piezoceramic vibrator was used to apply a load, where more than 10% of the acoustic energy was converted to electric power, nor did we detect a redshift when the water was stirred at a low amplitude of the acoustic waves, where sidebands were detected at not only low but also high frequencies. Therefore, we conclude that the redshift occurs through acoustic energy transfer to kinetic energy of the medium. We consider that the higher sidebands shown in Figs. 3(b) and 3(c) were caused by the streaming of the water.

In these experiments, the characteristics of the frequency spectrum depend on the position of the hydrophone in the experimental setup shown in Figs. 1 and 2. The redshift peak

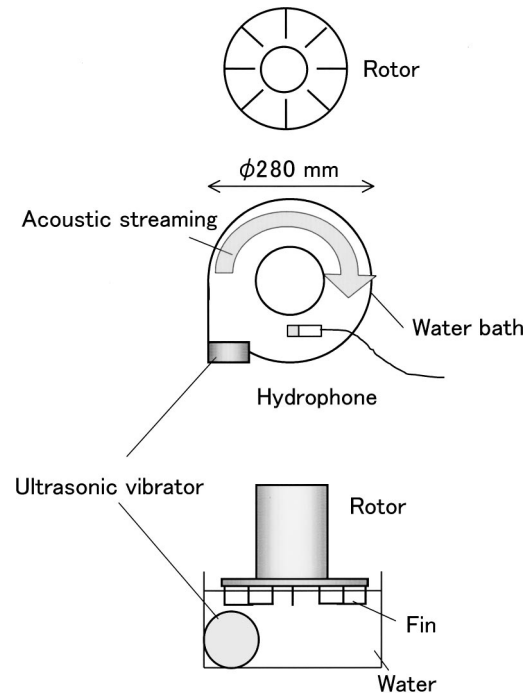


FIG. 2. Experimental setup for detecting the average velocity of acoustic streaming. The average velocity of water (volume of 2.7 l) is measured based on the rotation speed of a rotor. Water bath dimensions are 280 mm diameter and 50 mm depth. The rotor was driven by the streaming of the water; the driving force was received by the fins. The acoustic wave field was a standing wave field.

frequency is characteristically detected at the standing wave positions of nodes or antinodes, where the standing wave pitch is 0.75 mm at 1 MHz. We cannot at this stage obtain data that show backscattering, i.e., the characteristic of the redshift peak to depend on the direction of the hydrophone was not detected. (We did not detect the direction of the redshifted waves.)

We carried out experiments in an elliptic water pool ($10 \times 11 \text{ m}^2$, 2.5 m depth) to avoid the standing wave condition using continuous waves as shown in Fig. 6. The experimental setups were set to detect the backscattering of acoustic waves. The hydrophone was set parallel to the ultrasonic vibrator at a depth of 200 mm, and the experiments were performed changing the position of the ultrasonic vibrator. Figure 7 shows one of the typical results (the frequency is 1090 kHz and the electric input power is 130 W); the redshift peak is clearly shown. In these experiments, the redshift peak was always detected. We consider that the redshift peak in Fig. 7 is caused by backscattering of acoustic waves.

We carried out experiments in distilled degassed water to detect the influence of the bubbles. A redshift was not detected in distilled degassed water. We dissolved several types of powder in the degassed distilled water; a redshift was not detected in these experiments. We detected a redshift when contrast agents were dissolved in degassed distilled water. We tried to detect the Doppler shift of the moving medium using the present experimental setup. However, we could not detect the Doppler shift; we consider that the amplification of the present experimental setup was not enough. We conclude

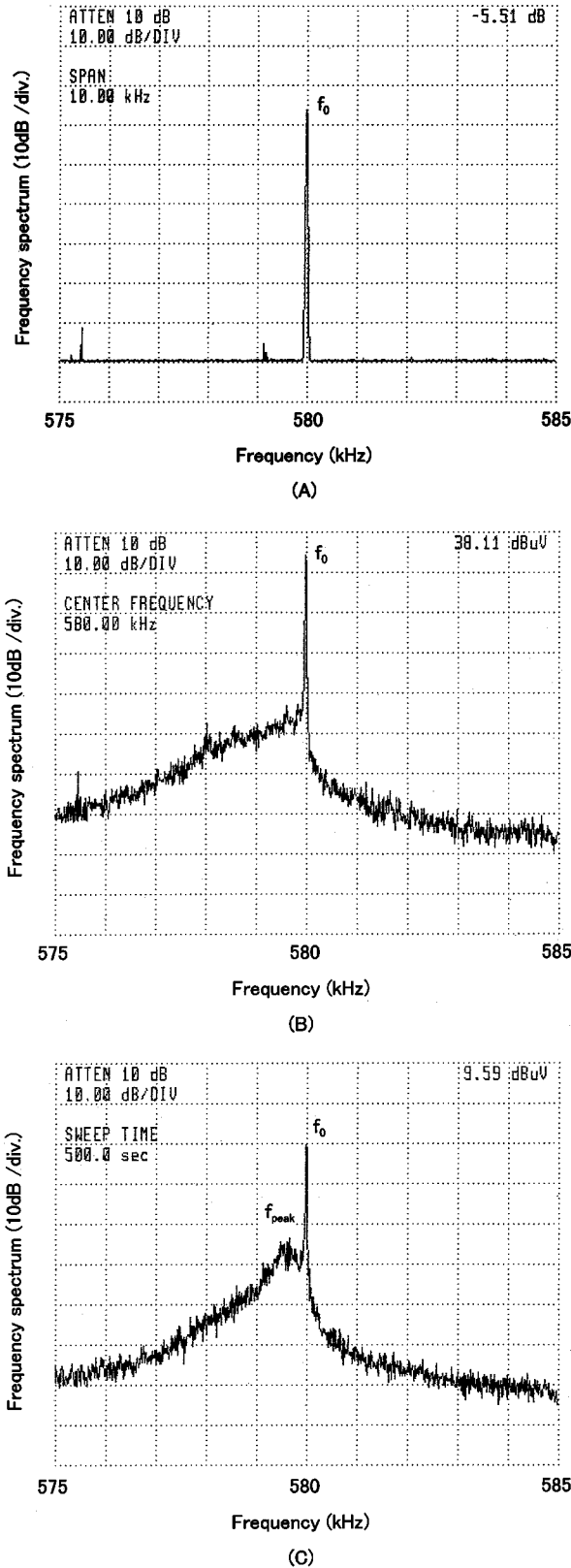


FIG. 3. Frequency spectrum of acoustic streaming in water. (a) $V_{in} = 9 V_{peak\ to\ peak}$: absence of acoustic streaming. (b) $V_{in} = 90 V_{peak\ to\ peak}$: redshift is detected. (c) $V_{in} = 90 V_{peak\ to\ peak}$: peak of the redshift frequency f_{peak} is detected. The difference in experimental conditions between (b) and (c) is the position of the hydrophone.

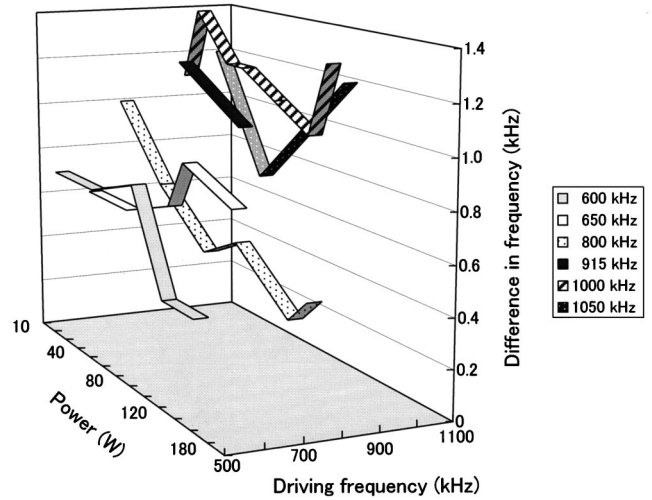


FIG. 4. $\Delta f_{peak} \equiv f_0 - f_{peak} = \Delta \omega_{peak} / 2\pi$ vs f_0 and P_0 , where f_0 is the driving frequency, f_{peak} is the redshift peak frequency, and P_0 is the input power. The three-dimensional figure shows that Δf_{peak} increases depending on the driving frequency f_0 and not on the input power P_0 .

that the level of the Doppler shift of a moving medium containing small powder or air bubbles was -30 to -40 dB less than the redshift.

III. DISCUSSION

A. Quantum-mechanical representation of acoustic waves

A quantum-mechanical representation of acoustic waves has been proposed [4–11]. Using the phonon density n_p , the energy density ε and momentum density μ are represented as

$$\varepsilon = n_p \hbar \omega, \tag{1}$$

$$\mu = n_p \hbar k. \tag{2}$$

Here, $\omega = 2\pi f$ (f is the frequency), $k = 2\pi/\lambda$ (λ is the wavelength) is the wave number, and $\hbar = h/2\pi$, where h is Planck’s constant.

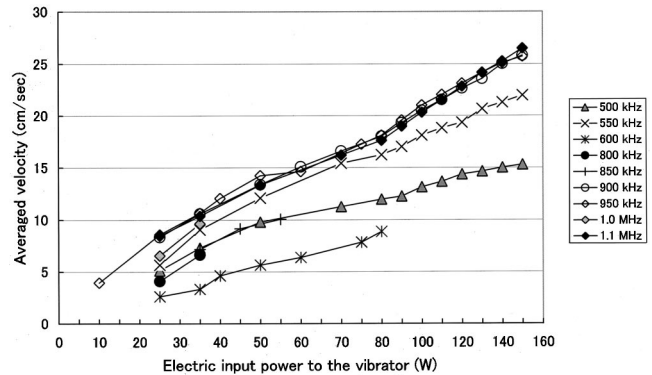


FIG. 5. Averaged velocity of acoustic streaming vs input power P_0 .

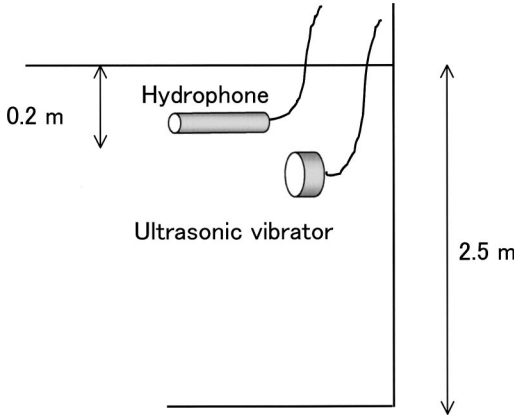


FIG. 6. Experimental setups in the elliptical water pool. The water pool is $10 \times 11 \text{ m}^2$ and 2.5 m deep. The hydrophone was set parallel to the ultrasonic vibrator at a depth of 200 mm, and the experiments were performed changing the position of the ultrasonic vibrator.

In acoustic streaming, the medium containing the acoustic waves is driven by the acoustic radiation pressure of the acoustic waves; thus the medium obtains kinetic energy from the acoustic waves.

B. Derivation of the driving force of acoustic streaming

The Hamiltonian density H is represented as the sum of the kinetic energy of unit volume $\rho \dot{x}^2/2$ and the acoustic energy density ε , as shown in Fig. 8 [9,11]. Here, ρ is the mass density and \dot{x} is the drift velocity of the medium, where the overdot indicates the time differential. The Hamiltonian density H is represented as

$$H = \frac{1}{2} \rho \dot{x}^2 + \varepsilon(x). \tag{3}$$

Using the momentum of the drifting medium, p_m , which is not equal to the momentum of the acoustic wave, μ , Eq. (3) can be rewritten as

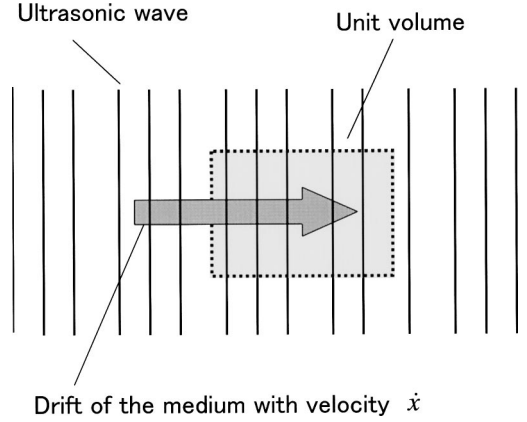


FIG. 8. Hamiltonian density. The Hamiltonian density is represented as the sum of the acoustic energy and the kinetic energy of the medium.

$$H = \frac{p_m^2}{2\rho} + \varepsilon(x). \tag{4}$$

Then, Hamilton’s canonical equations are derived as

$$\dot{x} = \frac{\partial H}{\partial p_m} = \frac{p_m}{\rho}, \tag{5}$$

$$\dot{p}_m = -\frac{\partial H}{\partial x} = -\frac{\partial \varepsilon}{\partial x}, \tag{6}$$

and therefore

$$\rho \ddot{x} = -\frac{\partial \varepsilon}{\partial x}. \tag{7}$$

Here, the energy density $\varepsilon = n_p \hbar \omega$, so that Eq. (7) can be rewritten as

$$\rho \ddot{x} = -\hbar \frac{\partial(n_p \omega)}{\partial x} = -\hbar \left(\omega \frac{\partial n_p}{\partial x} + n_p \frac{\partial \omega}{\partial x} \right). \tag{8}$$

Equation (8) indicates that not only the phonon density decrease ($\partial n_p / \partial x < 0$) but also the frequency decline ($\partial \omega / \partial x < 0$), which depends on distance x , produces the driving force for acoustic streaming.

C. Parametric down-conversion

In parametric decay, also known as the “three-wave interaction” or “down-conversion,” one wave decays into two waves, satisfying the energy and momentum conservation laws which are represented by Eqs. (9) and (10), respectively [3–11],

$$\omega_0 = \omega_1 + \omega_2, \tag{9}$$

$$\kappa_0 = \kappa_1 + \kappa_2. \tag{10}$$

Figure 9 shows the backscattering (reflection) of an acoustic wave by the medium and acoustic energy transfer to the kinetic energy of the medium, which causes the redshift. These phenomena occur when Eqs. (9) and (10) are satisfied; thus

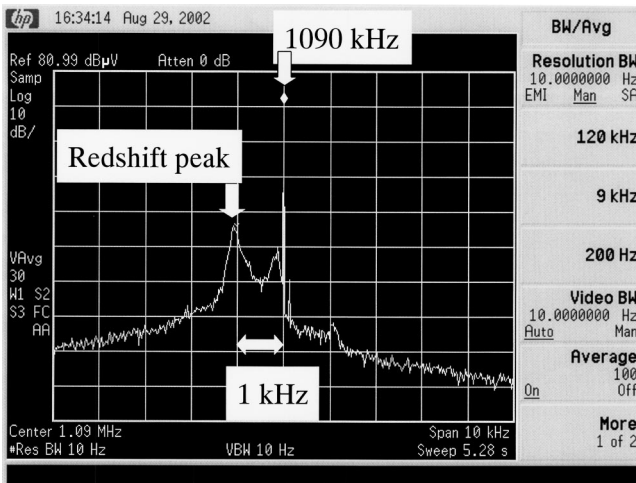


FIG. 7. Frequency spectrum in the elliptical water pool. Driving frequency is 1090 kHz and electric input power is 130 W.

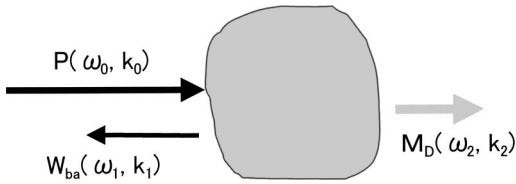


FIG. 9. Backscattering of an acoustic wave by the medium (acoustic energy reflection by the medium). The acoustic wave $P(\omega_0, k_0)$ decays into a backscattered acoustic wave $W_{ba}(\omega_1, k_1)$ and the kinetic motion of the medium $M_D(\omega_2, k_2)$; ω_2 and k_2 indicate the kinetic energy and momentum of the medium, respectively. A redshift indicates that the reflected wave frequency ω_1 is smaller than the longitudinal wave frequency ω_0 .

the parametric decay conditions are added that are represented on the frequency vs wave number (ω - k) diagram [4,8,16–19] shown in Fig. 10. Here, the straight lines Oa and Oa' show the dispersion relations of longitudinal waves. The ω axis represents the kinetic energy of the medium $\varepsilon_M = \rho\dot{x}^2/2$, and the k axis represents the momentum of the medium $\mu_M = \rho\dot{x}$. The quadratic curve m - 0 - m' shows the kinetic motion of the medium, which is represented by the momentum $\mu_M = \rho\dot{x}$ and the energy $\varepsilon_M = \rho\dot{x}^2/2$. The parallelogram OM_DPW_{ba} is the sufficient condition that shows energy and momentum conservation between the acoustic waves and the medium.

The backscattering mechanism is as follows: the acoustic wave represented as $OP(\omega_0, k_0)$ decays into a backscattered acoustic wave $OW_{ba}(\omega_1, k_1)$ and the kinetic motion of the medium represented as $OM_D(\omega_2, k_2)$; ω_2 and k_2 indicate the kinetic energy and momentum of the medium drift, respectively. The backscattering mechanism has a resonant frequency because the parallelogram OM_DPW_{ba} drawn in Fig.

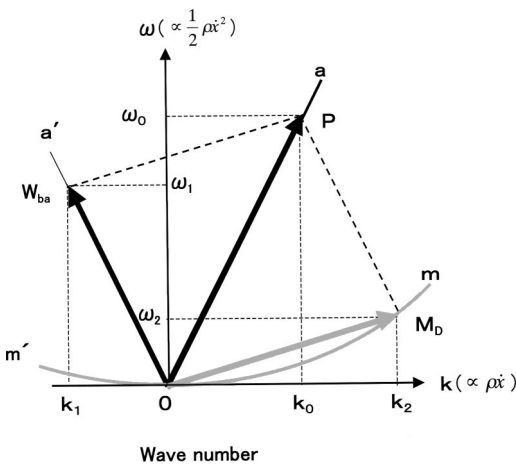


FIG. 10. Frequency vs wave number (ω - k) diagram of the redshift. The quadratic curve m - 0 - m' shows the kinetic motion of the medium, which is represented by the momentum $\mu_M = \rho\dot{x}$ and the energy $\varepsilon_M = (1/2)\rho\dot{x}^2$. The parallelogram OM_DPW_{ba} shows the sufficient conditions for acoustic wave transfer to the motion of the medium. The vector $OP(\omega_0, k_0)$ shows the acoustic wave, $OM_D(\omega_2, k_2)$ shows the medium drift, and $OW_{ba}(\omega_1, k_1)$ shows the backscattered acoustic wave, which is redshifted by $\omega_2 (= \omega_0 - \omega_1)$ from ω_0 .

10 is a sufficient condition for wave conversion (i.e., only the parallelogram OM_DPW_{ba} can be drawn in Fig. 10); therefore this condition determines the frequency of the backscattered acoustic wave ω_1 . Here, $\omega_0 > \omega_1 (= \omega_0 - \omega_2)$ indicates that the reflected waves are redshifted.

According to the explanation using the ω - k diagram, the difference between the driving frequency and the redshift peak frequency depends on the driving frequency; the difference in frequencies increases with the driving frequency. Figure 4 shows the averaged difference in frequencies depending on the driving frequency. We detected that the difference in frequencies increases with the driving frequency at 600–1000 kHz; however, at 1000–1050 kHz, the difference in frequencies decreases. The difference in frequency $\Delta f_{\text{peak}} = 1$ kHz at the driving frequency $f_0 = 1$ MHz; thus the redshift of $\Delta f_{\text{peak}}/f_0 = 0.1\%$ is equivalent to the Doppler shift caused by a sound source that leaves the hydrophone at a velocity of 0.75 m/s. We calculated the averaged drift velocity to be 0.25 m/s; however, there is a possibility that the peak drift velocity is 0.75 m/s at the focal point of the acoustic wave. At this stage, we have not detected the peak drift velocity. We also have not calculated the drift velocity that is derived from the matching conditions. In Sec. III E, we discuss the dissimilarity of the redshift peak from the Doppler shift.

D. Proposed mechanism for backscattering and redshift peak

In this section, a brief explanation of the mechanism of backscattering and acoustic streaming is given. We have shown the matching condition in Fig. 10, which indicated that not only a redshift but also backscattering is required. In Fig. 9, phonons are reflected elastically by the medium; thus a transfer of acoustic energy to the kinetic energy of the medium occurs. Here, “elastically” denotes complete acoustic energy transfer to the kinetic energy of the medium. In these discussions, the energy transfer from the acoustic wave to the thermal energy of the medium is not taken into account. These phenomena satisfy the energy and momentum conservation laws represented by Eqs. (9) and (10). Phonons are reflected by the medium; then the medium is caused to drift, which indicates that the reflection source is moving, and therefore the reflected waves undergo a Doppler shift. This explanation is valid only for the redshift peaks, because the redshift frequency is determined by the condition represented by the parallelogram OM_DPW_{ba} in Fig. 10. The difference in frequency does not depend on the electric input power, but the averaged drift velocity does; this indicates that the difference in frequency does not depend on the velocity of the medium drift. Therefore, we find it difficult to explain redshift as a Doppler shift. We also detected a redshift broadband, which increases according to the electric input power, as discussed in Sec. III D; however, we cannot at this stage completely explain the mechanism of broadband frequency decline. In this argument, it is assumed that the energy transfer satisfies the momentum conservation law between an acoustic wave and the medium.

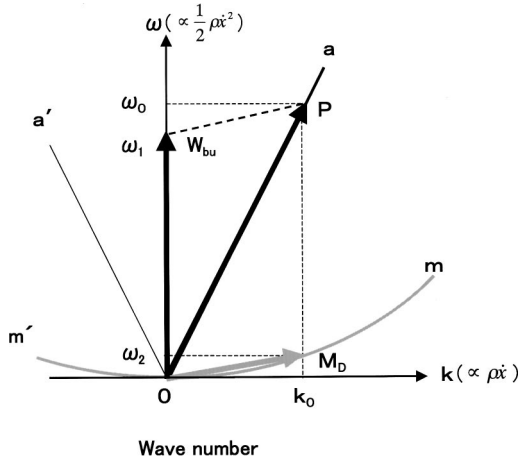


FIG. 11. ω - k diagram of acoustic wave absorption by bubbles. The longitudinal wave $OP(\omega_0, k_0)$ decays into bubble oscillations $OW_{bu}(\omega_1, k_1)$ and motion of the medium (i.e., bubble drift motion) $OM_D(\omega_2, k_2)$, where the vector $OW_{bu}(\omega_1, k_1)$ indicates redshifted spherical bubble oscillations. The frequency of the longitudinal waves is redshifted from ω_0 to ω_1 ($< \omega_0$) of the bubble oscillations.

We consider that the redshift peak in Fig. 7 is caused by the backscattering of acoustic waves. Both a peak redshift and a peak blueshift are shown in Fig. 7. The blueshift peak is 30 dB down compared with the redshift peak. We consider that we detected not only the redshift component but also the Doppler shift of the vortex motion. However, at this stage we cannot separate the Doppler shift of the vortex motion and the redshift component.

E. Proposed mechanism for redshift peak

The redshift peaks were position dependent; thus we propose another mechanism for them. If there are bubbles, the longitudinal wave may decay into bubble oscillations and motion of the medium. Figure 11 shows an ω - k diagram where the longitudinal wave $OP(\omega_0, k_0)$ decays into bubble oscillations $OW_{bu}(\omega_1, k_1)$ and motion of the medium $OM_D(\omega_2, k_2)$. In bubble oscillations, the mean value of the wave number along the propagation direction of the longitudinal wave is 0; therefore the bubble oscillations are represented as the point $W_{bu}(\omega_1, k_1=0)$ on the ω axis. The par-

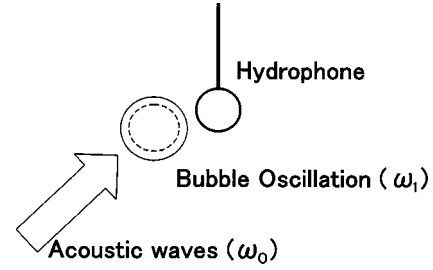


FIG. 12. Bubble oscillation. The pressure fields due to bubbles oscillating symmetrically decay with radial distance r as r^{-2} . Therefore, the oscillation can be detected when the hydrophone is in direct contact with the bubbles or the near field of the bubbles.

allelogram OM_DPW_{bu} shows the matching condition where the vector OW_{bu} indicates spherical bubble oscillations whose frequency is redshifted. The frequency of longitudinal waves is redshifted from ω_0 to ω_1 ($< \omega_0$) of the bubble oscillations. Furthermore, the pressure fields due to bubbles oscillating symmetrically decay with radial distance r as r^{-2} [20]. Therefore, as shown in Fig. 12 the oscillation can be detected when the hydrophone is in direct contact with the bubbles or the near field of the bubbles. This is why the peak frequency component is detected depending on the position of the hydrophone.

IV. CONCLUDING REMARKS

We investigated acoustic waves from the viewpoints of energy and momentum. A redshift of the acoustic wave frequency is observed in acoustic streaming. We showed that there are two types of redshift mechanism. One is bubble oscillation and the other is backscattering. We can show sufficient conditions for redshift using the ω - k diagram; however, we cannot illustrate the mechanism. At this stage we could not explain the phenomena using hydrodynamics or kinetic theory. Therefore, we attempted to apply quantum mechanics for the explanation of redshift. However, we believe that classical theory will explain the phenomena.

ACKNOWLEDGMENT

We thank Y. Oiwa (Toyota National College of Technology) for technical support.

- [1] H. J. Maris, Phys. Rev. A **8**, 2629 (1973).
- [2] J. S. Foster and S. Putterman, Phys. Rev. Lett. **54**, 1810 (1985).
- [3] I. L. Bajak and M. A. Breazeale, J. Acoust. Soc. Am. **68**, 1245 (1980).
- [4] M. Sato and T. Fujii, Jpn. J. Appl. Phys., Part 1 **36**, 2959 (1997).
- [5] M. Sato, K. Matsuura, and T. Fujii, J. Chem. Phys. **114**, 2382 (2001).
- [6] M. Sato, N. Shibuya, N. Okada, T. Tou, and T. Fujii, Phys. Rev. E **65**, 046302 (2002).
- [7] M. Sato and T. Fujii, in *IEEE Ultrasonics Symposium Proceed-*

ings, Sendai, Japan, 1998, Vol. 2 (IEEE, Sendai, 1998), pp. 1187–1192.

- [8] M. Sato and T. Fujii, Phys. Rev. E **64**, 026311 (2001).
- [9] M. Sato, H. Sugai, and T. Fujii, J. Acoust. Soc. Jpn. **53**, 352 (1997) (in Japanese).
- [10] M. Sato and T. Fujii, J. Acoust. Soc. Jpn. **53**, 359 (1997) (in Japanese).
- [11] M. Sato, H. Itoh, and T. Fujii, Ultrasonics **38**, 312 (2000).
- [12] O. V. Rudenko and S. I. Soluyan, *Theoretical Foundations of Nonlinear Acoustics* (Consultants Bureau, New York, 1977), pp. 187–211.

- [13] T. G. Leighton, *The Acoustic Bubble* (Academic, San Diego, 1997), pp. 56–58.
- [14] O. V. Rudenko, A. P. Sarvazyan, and S. Y. Emelianov, *J. Acoust. Soc. Am.* **99**, 2791 (1996).
- [15] A. A. Donikov, *J. Acoust. Soc. Am.* **103**, 143 (1998).
- [16] F. F. Chen, *Introduction to Plasma Physics* (Plenum, New York, 1974), p. 259.
- [17] L. H. Taylor and F. R. Rollins, Jr., *Phys. Rev.* **136**, 591 (1964).
- [18] F. R. Rollins, Jr., L. H. Taylor, and P. H. Tood, Jr., *Phys. Rev.* **136**, 597 (1964).
- [19] C. F. Quate and R. B. Thompson, *Appl. Phys. Lett.* **16**, 494 (1970).
- [20] M. S. Longuet-Higgins, *J. Fluid Mech.* **201**, 525 (1989).